



OPEN ACCESS

EDITED BY

Meng Zheng,
Qingdao Haiwan Science and
Technology Industry Research Institute
Co., Ltd., China

REVIEWED BY

Zhemi Xu,
Beijing Technology and Business
University, China
Chuanyu Sun,
University of Padua, Italy

*CORRESPONDENCE

M. Wang,
✉ wangming@lntu.edu.cn

SPECIALTY SECTION

This article was submitted to
Electrochemistry,
a section of the journal
Frontiers in Chemistry

RECEIVED 01 December 2022

ACCEPTED 27 February 2023

PUBLISHED 09 March 2023

CITATION

Li W, He Y, Bao WB, Bao HL, Li DY,
Zhang CL and Wang M (2023), Novel
TiO₂/GO/M-MMT nano-
heterostructured composites exhibiting
high photocatalytic activity.
Front. Chem. 11:1113186.
doi: 10.3389/fchem.2023.1113186

COPYRIGHT

© 2023 Li, He, Bao, Bao, Li, Zhang and
Wang. This is an open-access article
distributed under the terms of the
[Creative Commons Attribution License
\(CC BY\)](https://creativecommons.org/licenses/by/4.0/). The use, distribution or
reproduction in other forums is
permitted, provided the original author(s)
and the copyright owner(s) are credited
and that the original publication in this
journal is cited, in accordance with
accepted academic practice. No use,
distribution or reproduction is permitted
which does not comply with these terms.

Novel TiO₂/GO/M-MMT nano-heterostructured composites exhibiting high photocatalytic activity

W. Li¹, Y. He², W. B. Bao¹, H. L. Bao², D. Y. Li², C. L. Zhang² and
M. Wang^{2*}

¹School of Architecture and Civil Engineering, Shenyang University of Technology, Shenyang, Liaoning, China, ²School of Materials Science and Engineering, Liaoning Technical University, Fuxin, Liaoning, China

This study proposed a technique to enhance the photocatalytic properties of TiO₂ using graphene oxide (GO) and modified Montmorillonite (M-MMT). TiO₂/GO/M-MMT nano-heterostructured composites were prepared *via* hydrothermal and co-precipitation. The photocatalytic performance was evaluated by investigating the photodegradation rate and absorption behavior of methyl orange (MO) under visible light irradiation. The results showed that TiO₂/GO/M-MMT heterojunction exhibited excellent photocatalytic degradation performance, as the degradation rate of MO was observed to be 99.3% within 150 min. The density of adsorbed MO decreased by 62.1% after 210 min of dark adsorption using the TiO₂/GO/M-MMT composite, which was significantly higher than that achieved using M-MMT, GO/M-MMT, and TiO₂/M-MMT. The nano-heterostructure increased the effective interface between TiO₂, GO, and MMT, which increased the charge transfer ability and prolonged the electron-hole separation time. Therefore, the results of this study can be used to design novel photocatalysts to eradicate environmental pollutants.

KEYWORDS

TiO₂/GO/M-MMT composite, methyl orange, photocatalytic performance, electron transfer ability, nanoheterostructures

1 Introduction

Environmental pollution engendered from rapid advancements in the modern chemical industry has attracted the attention of researchers worldwide. Secondary chemical contamination can be caused during the degradation of pollutants using chemical methods (Laysandra et al., 2017). Photocatalytic degradation has been used to eradicate organic pollutants from wastewater owing to its several advantages such as operation simplicity, low cost and pollution-free nature (Lee et al., 2018; El-Kousy et al., 2020; Dao et al., 2021; Liu et al., 2022).

Titanium dioxide (TiO₂) is one of the most efficient photocatalysts used to produce hydrogen owing to its low cost, high stability, corrosion resistance, and environmental friendliness (Tao et al., 2020; Wang et al., 2021). TiO₂ photocatalysts have been used for industrial wastewater treatment using solar energy by converting the wastewater into non-toxic chemical products without producing any other pollutants. However, because of the wide band gap, TiO₂ must be irradiated with ultraviolet light, which constitutes approximately only 4% of visible light and provides low quantum yield (Wang et al.,

2019). TiO₂ activity can be enhanced by coupling it with other semiconductors or doping with higher work-function metals (Yadav and Ahmad, 2015; Umer et al., 2019; Yang et al., 2020; Xiang et al., 2021; Li et al., 2022a; Dong et al., 2022; Jing et al., 2022; Xu and Li, 2022). Montmorillonite (MMT) is the most widely used material in clay semiconductor nanocomposites owing to its layered structure, high cation exchange capacity, excellent charge trapping ability, and considerable adsorption potential for semiconductor particles (Wang et al., 2011; Paiva et al., 2014; Sharma et al., 2018). Clay-TiO₂/MMT heterostructured composites can provide additional number of sites for trapping photo-generated electrons, which ultimately enhances the photocatalytic activity (Liao et al., 2022; Wang et al., 2022). Additionally, graphene oxide (GO) can enhance the catalytic effect of semiconductors (Joshi et al., 2020) and can be used to provide electric carriers with more active attachment-sites for photocatalysis. This enables a faster transfer of photoelectrons, avoids accumulation because of its high electrical conductivity and large specific surface area, thereby reducing the possibility of electron-hole recombination. Liu et al. (2021) prepared N-TiO₂/GO photocatalyst *via* sol-gel and hydrothermal methods and analyzed its adsorption performance for RhB.

Photocatalysis is a new, efficient and potential discovery. It uses renewable energy to decompose organic pollutants by sunlight. At present, the known photocatalytic materials are semiconductor materials and polymer materials. In the past decade, polymer photocatalysts have been developed rapidly, and many polymer photocatalysts with catalytic activity have been found (Kumar et al., 2021; Nadali et al., 2021; Yin et al., 2022). However, polymer photocatalysts have limited photochemical stability, lack of understanding of the reaction mechanism, balance between charge carrier lifetime and catalytic time, and the use of unsustainable sacrificial reagents (Tahir, 2017; Dao et al., 2021). However, the photocatalytic performance of TiO₂/GO/MMT nanoheterostructured composite has not been reported thus far. In this study, a TiO₂/GO/MMT nanocomposite was synthesized *via* hydrothermal and co-precipitation methods and the photodegradation of methyl orange (MO) using the nanocomposite was studied.

2 Experimental process

Modified MMT (M-MMT; 1 g) and cetyltrimethylammonium bromide (CTAB; 1 g) (~1% of MMT mass) were added to distilled water (200 mL) under ultrasonic conditions for 60 min. A certain amount of GO [prepared *via* the modified Hummer method (Pu et al., 2019)] was added to the M-MMT solution and stirred for 12 h using a magnetic stirrer. The solution was kept idle at room temperature for 24 h. Subsequently, the precipitates were washed, dried, and grinded to obtain the GO/M-MMT composite.

CTAB and butyl titanate were weighed at a ratio of 1:2 ($n_{\text{CTAB}}/n_{\text{Ti}} = 0.5$). The CTAB was then dispersed in 30 mL of distilled water and butyl titanate was placed in a beaker. A certain amount of the GO/M-MMT composite was added to the CTAB solution. After stirring for 30 min, butyl titanate was dropped into the solution at a rate of 0.5 drop/s using a dropper. After titration, the as-prepared solution was poured into a reactor and hydrothermally treated at 180°C for 10 h. A white powder was obtained after filtration and

drying. The composite, TiO₂/GO/M-MMT, was obtained by calcining the powder at 300°C for 50 min in a muffle furnace.

The microstructure of the TiO₂/GO/M-MMT composite was analyzed *via* scanning electron microscopy (SEM) (JSM-7500F) and X-ray diffraction (XRD) (Shimadzu 6100). The atom bonding situation, specific surface area, and pore distribution of the TiO₂/M-MMT, TiO₂/GO, and TiO₂/GO/M-MMT composites were measured using X-ray photoelectron spectroscopy (XPS) (Shimadzu/Kratos Axis Ultra DLD) and the BET (ASAP 2460) method.

The irradiation light power is 1380 W/m². The wavelength range of visible light is 400–760 nm. Visible light is used to study the photocatalytic performance in the experiment. The rate of photodegradation was tested using a 722S visible spectrophotometer. The photocatalytic performance of the composite was evaluated directly by measuring the change in the rate of degradation MO. The initial absorbance of MO (denoted by A₀) without the catalyst before illumination was determined by adjusting the wavelength. First, the suspension was stirred in dark for 60 min to achieve an adsorption–desorption equilibrium, and the solution was sampled every 20 min during the experiment. Next, the samples were centrifuged for 5 min at a speed of 4000 rpm using a high-speed centrifuge, following which the supernatant was collected to measure the absorbance (denoted by A). The following equation (Eq. 1) was used to calculate the degradation rate (η).

$$\eta = \frac{A_0 - A}{A_0} \times 100\% \quad (1)$$

The composite (0.05 g) was placed in a MO solution (100 mL, 10 mg/L). The solution was irradiated with ultraviolet light and stirred in a dark box for 40 min. After centrifugation, the absorbance of the MO solution was measured at a wavelength of 460 nm. The amount of MO adsorbed by the composite was calculated using the following equation (Eq. 2).

$$q_t = \frac{(C_0 - C_t)V}{W} \quad (2)$$

where q_t , V , and W represent the amount of MO adsorbed (mg/g), initial volume of the MO solution (L), and the quantity of the composite (g), respectively. C_0 and C_t denote the initial density (mg/L³) and the concentration of the MO solution (mg/L) at time t , respectively.

The activity of TiO₂/GO/M-MMT photocatalyst will be evaluated by the change of methyl orange concentration and its adsorption capacity. At the same time, the pseudo-first-order kinetic equation will be given to further study the kinetics of photocatalytic degradation, and the mechanism of photocatalytic degradation will be discussed.

3 Results and discussion

Figure 1A shows the image of M-MMT, which displays a layered structure. Figure 1B shows the morphology of the GO/M-MMT composite. Several layers of the GO sheets are rough and wrinkled, which might provide more active sites for other components (TiO₂). As can be observed from Figure 1C, several small and uniform TiO₂

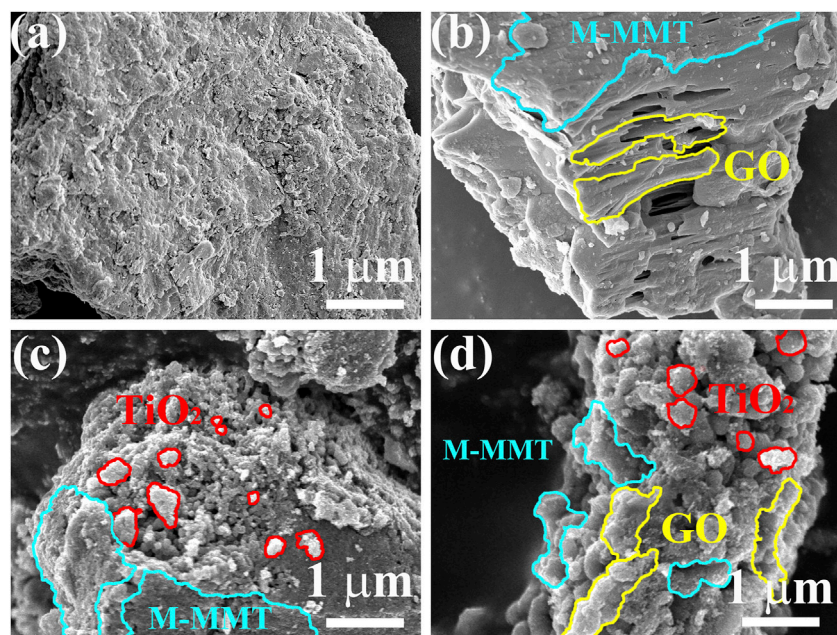


FIGURE 1
Scanning electron microscope images of different specimen. (A) M-MMT; (B) GO/M-MMT; (C) TiO_2 /M-MMT; (D) TiO_2 /GO/M-MMT.

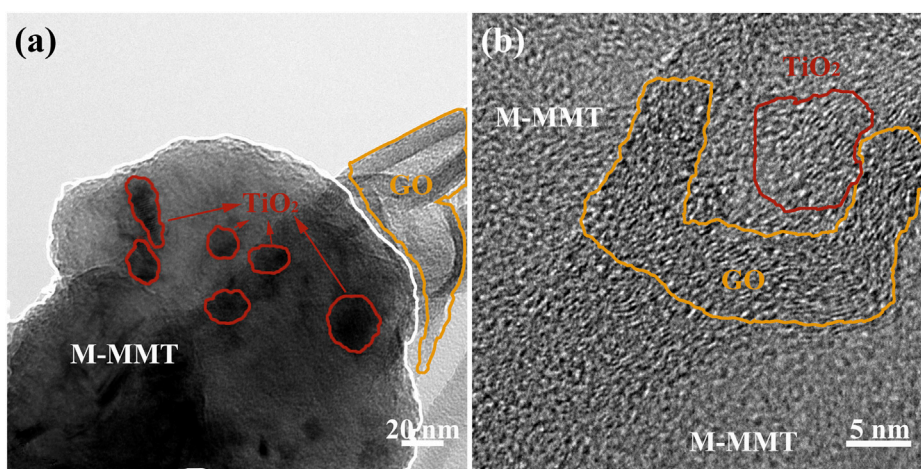


FIGURE 2
(A) The TEM images of TiO_2 /GO/M-MMT nanocomposites; (B) The HRTEM image of TiO_2 /GO/M-MMT composites.

particles are formed on the surface of M-MMT, which is expected to improve the catalytic performance of the composite. The SEM images of the TiO_2 /GO/M-MMT nanocomposite (Figure 1D) reveals that several uniform-sized TiO_2 nano-particles and layered GO sheets are formed on the M-MMT surface.

The energy dispersive X-ray spectroscopy results for the TiO_2 /GO/M-MMT nanocomposite (Supplementary Figure S1) reveal that Al, Si, C, O, and Ti are distributed on the TiO_2 /GO/M-MMT nanocomposite, indicating that TiO_2 , GO, and M-MMT form a uniform compound structure. The composition of the composite is

illustrated further in the inset of Supplementary Figure S1B. The amounts of O, C, Si, Al, and Ti are reported as 21.51%, 73.00%, 0.06%, 0.05%, and 5.38%, respectively.

The TEM images of TiO_2 /GO/M-MMT nanocomposites in Figure 2A, GO is circled by the orange ring, M-MMT is circled by the white line. The growth on M-MMT is TiO_2 , which is marked with a red circle. In the figure, it can be seen that the large layer M-MMT and TiO_2 particles are tightly wrapped with the film GO, and the TiO_2 particles with a diameter of 15–20 nm grow uniformly on the M-MMT, which is consistent with the SEM in Figure 1D. The

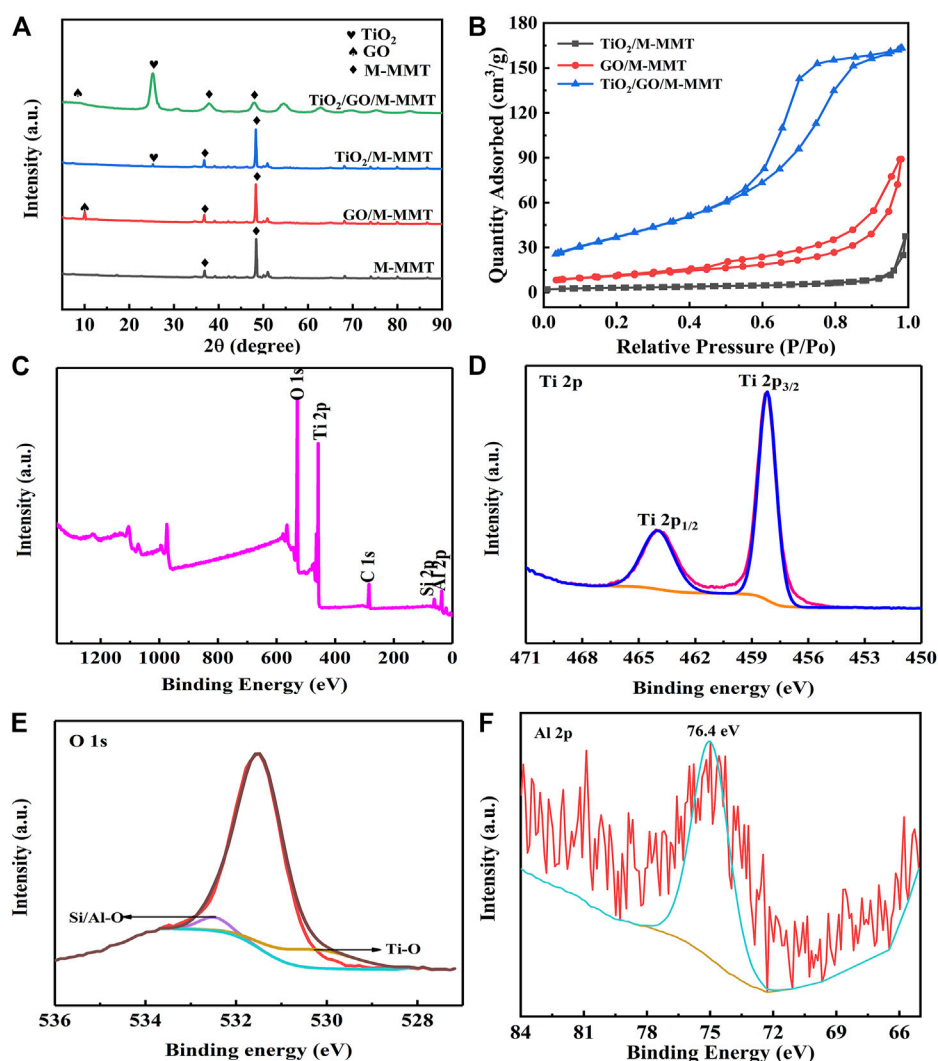


FIGURE 3

(A) X-ray diffraction patterns of different specimen with M-MMT, GO/M-MMT, TiO₂/M-MMT and TiO₂/GO/M-MMT; (B) Nitrogen adsorption and desorption curve of different nanocomposite; (C) XPS full spectrum of TiO₂/GO/M-MMT and high resolution XPS spectrum of (D) Ti 2p; (E) O 1s; (F) Al 2p.

HRTEM image of TiO₂/GO/M-MMT composites is shown in Figure 2B, in which the lattice fringes of TiO₂ and GO can be clearly detected. The d spacing of GO is 0.38 nm, which is wider than that of Graphene. The reason for this phenomenon is that oxygen enters the interlayer of graphene, increasing the distance between the surfaces of graphene. The d spacing of TiO₂ is 0.35 nm, corresponding to the (101).

The XRD patterns obtained for M-MMT, GO/M-MMT, TiO₂/M-MMT, and TiO₂/GO/M-MMT are shown in Figure 3A. The XRD patterns obtained for M-MMT display a weak diffraction peak near 7°, which corresponds to the (100) characteristic diffraction peak of M-MMT. In addition to the characteristic M-MMT peaks, the GO/M-MMT spectrum displays an additional strong diffraction peak at 10°, which corresponds to the (002) characteristic peak of GO. A weak diffraction peak is observed in the TiO₂/M-MMT spectrum at 25.5°, corresponding to the (101) peak of TiO₂. Diffraction peaks corresponding to GO and TiO₂ are observed in the spectrum of TiO₂/GO/M-MMT. The diffraction-peak intensity corresponding to

TiO₂ is higher than that corresponding to TiO₂/M-MMT. In TiO₂/M-MMT, the ratio of M-MMT is much higher than that of TiO₂, the grains are closely arranged in the same direction and the crystallinity is better in the diagram, which makes the intensity of the M-MMT diffraction peak is higher than that of others. The higher diffraction peak shows that the TiO₂ diffraction peak is very small. In TiO₂/GO/M-MMT composites, the addition of GO makes it enter into the layered M-MMT layers, which changes the distance between layers, so that the diffraction peak of M-MMT becomes shorter and wider, and the intensity of TiO₂ diffraction peak increases after data normalization; however, the peak at 25.5° shifts to a lower angle. Because the M-MMT load is a lamellar structure, the layer spacing becomes wider because the addition of TiO₂ and GO enter the interlayer. According to the Bragg equation $2d\sin\theta = n\lambda$, the value of d increases and the value of θ decreases. The diffraction peak of M-MMT is relatively weak, indicating that TiO₂ is attached to the surface of M-MMT. In addition, the diffraction peak of the composite is broadened. This could be because TiO₂ and GO entered the M-MMT interlayer *via* intercalation.

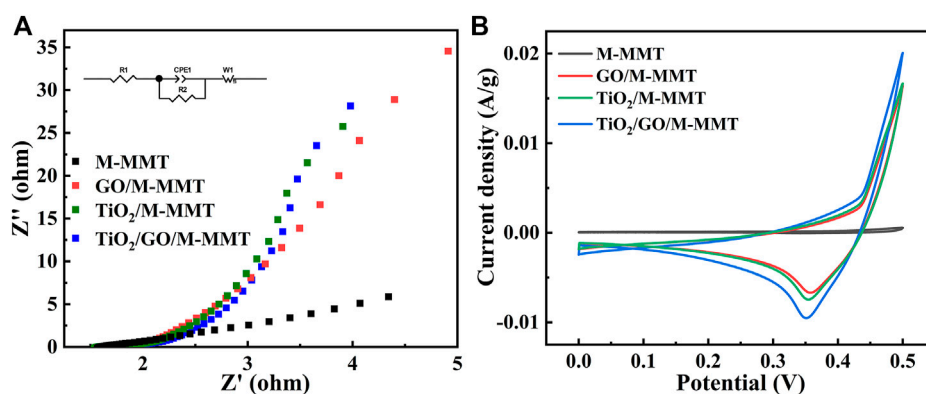


FIGURE 4

(A) EIS Nyquist plots of M-MMT, GO/M-MMT, TiO₂/M-MMT and TiO₂/GO/M-MMT nanocomposite; (B) Current-potential plots of different nanocomposite.

Figure 3B shows the specific surface area of the GO/M-MMT, TiO₂/M-MMT, and TiO₂/GO/M-MMT nanocomposites. The specific surface area of TiO₂/M-MMT, GO/M-MMT, and TiO₂/GO/M-MMT nanocomposites were measured as 12 m²/g, 42 m²/g, and 117 m²/g, respectively. The specific surface area of the TiO₂/GO/M-MMT composite is approximately ten and three times higher than that of TiO₂/M-MMT and GO/M-MMT, respectively. The large specific area opened more number of ion-transportation channels, resulting in a faster electron transport rate and more number of adsorption active sites, thereby improving the photocatalytic performance. Supplementary Figure S2 shows the pore-size distributions of the GO/M-MMT, TiO₂/M-MMT, and TiO₂/GO/M-MMT nanocomposites, which have average pore sizes of 6.7, 9.2, and 13.4 nm, respectively. The average pore size of the TiO₂/GO/M-MMT nanocomposite is the highest, indicating that the ion transport channels become wider, resulting in higher electron transport rates and photocatalytic degradation rates (Kočič et al., 2014; Mottola et al., 2022).

The characteristic peaks of Al, Si, C, Ti, and O are observed in the XPS full spectrum of the TiO₂/GO/M-MMT nanocomposite (Figure 3C). The peaks of 458.6 and 464.4 eV observed in the Ti 2p high-resolution spectrum (Figure 3D) can be attributed to Ti 2p_{3/2} and Ti 2p_{1/2}, respectively, indicating that Ti bonded to oxygen and exhibited a +4 valence in the composites. The O 1s peak is separated and fitted as shown in Figure 3E. The peaks at 531.5, 532.0, and 532.5 eV correspond to the O–O, Ti–O, and Si/Al–O bonds, respectively. The characteristic peak at 74.6 eV in the Al 2p XPS profile (Figure 3F) represents the Al–O bond in M-MMT.

Figure 4A shows EIS Nyquist plots of different composites. Because M-MMT is a natural mineral material, the conductivity is weak and the slope is low. With the addition of GO and TiO₂, the conductivity is improved, and the slope is increased. In TiO₂/GO/M-MMT nanocomposites, due to the synergistic effect of GO and TiO₂, the separation of electron-hole pairs is accelerated and the lifetime of photoinduced carriers is prolonged, thus enhancing the photocatalytic activity. The conductivity is enhanced, and the slope value is gradually close to 1, showing strong conductivity. Figure 4B shows the current-potential curves of different composites. The area enclosed by the CV curve is the activity of the material, and the more active the photocatalytic

performance is. The CV curve of M-MMT in the diagram is almost a straight line, and the macroscopic performance is poor catalytic performance. In GO/M-MMT and TiO₂/M-MMT, with the addition of GO and TiO₂ to M-MMT, the activity gradually increased and the reduction peak appeared. In TiO₂/GO/M-MMT, the area is the largest, the position of the reduction peak is the lowest, and the activity is the best, indicating that its photocatalytic performance is the best.

Figure 5A shows the rate of degradation of MO using the photocatalysts prepared in the study. The degradation test conducted for 240 min reveals that the rate of degradation of MO using M-MMT is only 15%. As the amounts of GO and TiO₂ increase, the rate of degradation of MO increases to 41% and 79%, respectively. With the TiO₂/GO/M-MMT nanocomposite, the rate of degradation of MO is 99%, which is twice as high as that achieved with GO/M-MMT. These results indicate that the TiO₂ component plays an important role in the MO degradation process.

Figure 5B shows the adsorption performances of the M-MMT, GO/M-MMT, TiO₂/M-MMT, and TiO₂/GO/M-MMT nanocomposites for MO. After the visible-light illumination, the adsorption performance of the composites TiO₂/M-MMT and GO/M-MMT are superior to that of M-MMT. The TiO₂/GO/M-MMT nanocomposite exhibits the highest adsorption capacity. The higher photocatalytic activity of the TiO₂/GO/M-MMT nanocomposite is attributed to the presence of the M-MMT component, which improves the dispersion ability of the photocatalyst and enhances the adsorption capacity for photons and MO molecules in the composites. Further, the addition of TiO₂ and GO extends the response range for visible light, thereby effectively reducing the recombination rate of electric carriers (Lin et al., 2020; Xiang et al., 2021).

The kinetics of the photocatalytic degradation was studied further to investigate the mechanism of the photocatalytic degradation. A pseudo-first-order kinetic equation is given in the following equation (Eq. 3) (Sharma et al., 2018).

$$\ln(C_0/C_t) = kt \quad (3)$$

where k is the quasi-first-order reaction rate constant (min⁻¹) and t is the irradiation time (min).

Figure 5C shows the change in the concentration of MO after adsorption using the different composites. For all composites, the concentration of MO decreases after adsorption. The change in the

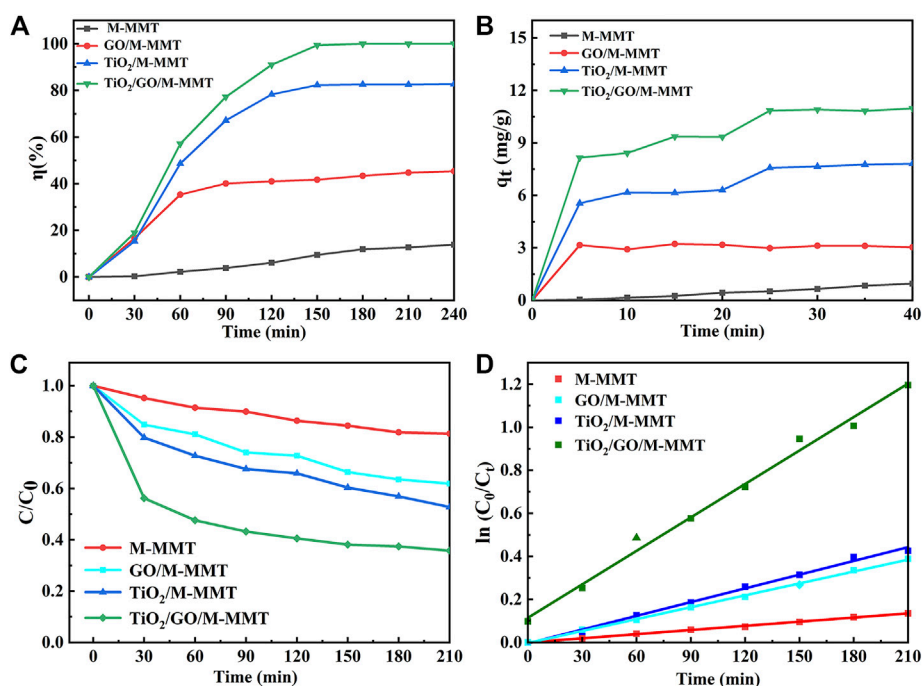
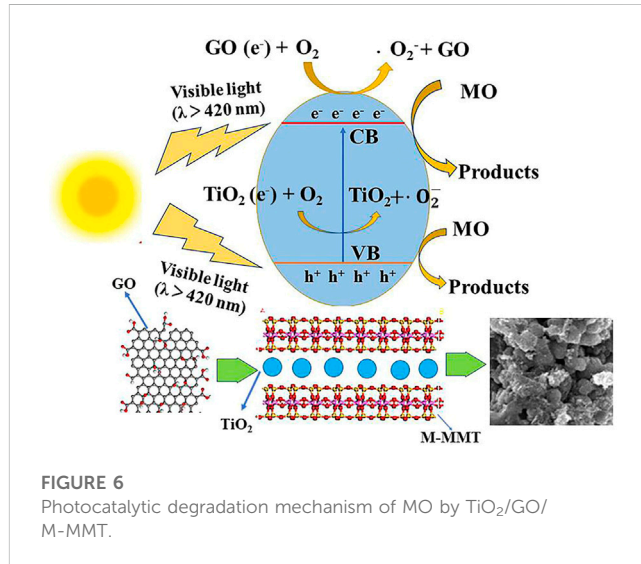


FIGURE 5

Photocatalytic performance curve of different photocatalyst. (A) The photocatalytic degradation rate curve; (B) The adsorption capacity curve; (C) Photodegradation concentration curve of MO; (D) Pseudo-first-order kinetic equation fitting diagram of different nanocomposite.

concentration of MO observed after adsorption achieved with the M-MMT photocatalyst is small; however, the concentration considerably decreases after adsorption achieved with TiO₂/GO/M-MMT. The TiO₂/GO/M-MMT system can produce higher yield of $\bullet\text{O}_2^-$, which generate more other active species and sites. Accordingly, the TiO₂/GO/M-MMT composite had a high photocatalytic performance with excellent stability and can be recommended for removing the antibiotic compounds. The concentration of MO with different adsorption times is fitted for different photocatalysts, as shown in Figure 5D. The k value estimated for M-MMT is observed to range from minimum to zero, indicating a weak response to visible light. The k value for the TiO₂/M-MMT nanocomposite is higher than that of the GO/M-MMT nanocomposite, indicating that the response time of TiO₂/M-MMT to visible light is longer than that of GO/M-MMT. The degradation rate can be significantly increased using a combination of the three components (the k value increases). GO can reduce the space charge region of TiO₂ and induce its electric field to separate photogenerated carriers effectively, which increases the photocatalytic activity. However, when the space charge region becomes too narrow, the dopant concentration increases and the recombination of photogenerated carriers becomes faster (Lincho et al., 2021; Olea et al., 2021; Li et al., 2022b).

According to experimental results explained above, the mechanism of the photocatalytic degradation of MO using TiO₂/GO/M-MMT is proposed, as shown in Figure 6. When the MO dyes are irradiated with visible light, the MO dyes become photosensitized and initiate the photocatalytic process. Visible light is absorbed by the photosensitized



MO dye molecules, which excites the MO-dye electrons to a higher energy level. Furthermore, the light-triggered electrons are transported from the high-energy state to the conduction band of TiO₂, and MO is degraded by the active TiO₂. Moreover, some electrons are transferred from TiO₂ to GO. Because the two-dimensional π -conjugated structure in GO is the electron acceptor, this special structure can effectively suppress the recombination between charges and carriers. The recombination between the light-triggered electrons and oxygen produces superoxide radicals ($\bullet\text{O}_2^-$) (Tahir, 2017). MO dye molecules are oxidized by these superoxide radicals to produce CO₂,

H₂O, and intermediates. In addition, the layered structures of M-MMT enhance the adsorption capacity of the composites, which improve the photocatalytic performance (Chen et al., 2018; Yang et al., 2019; Foroutan et al., 2020; Mallik et al., 2021).

4 Conclusion

To promote the uniform dispersion of nano-TiO₂ and improve the adsorption capacity of the photocatalyst, TiO₂/GO/M-MMT nanocomposites were prepared. The main conclusions are as follows:

- 1) The interlayer space in the nanocomposites increased with the addition of GO, providing more space for TiO₂ to enter the interlayer. The uniform nano-sized TiO₂ particles were distributed in the interlayer and on the surface of the TiO₂/GO/M-MMT nanocomposite, which formed ideal nanostructures.
- 2) The photocatalytic degradation rate of MO by the TiO₂/GO/M-MMT nanocomposite was up to 99.3%. The nanocomposite exhibited a better adsorption performance, which conformed to the pseudo-first-order kinetic equations.

Data availability statement

The original contributions presented in the study are included in the article/[Supplementary Material](#), further inquiries can be directed to the corresponding author.

Author contributions

WL: designing and completing experiments, writing—original draft. WB: investigation, writing—review. YH, HB, DL, and CZ:

References

- Chen, G.-G., Hu, Y.-J., Peng, F., Bian, J., Li, M. F., Yao, C. L., et al. (2018). Fabrication of strong nanocomposite films with renewable forestry waste/montmorillonite/reduction of graphene oxide for fire retardant. *Chem. Eng. J.* 337, 436–445. doi:10.1016/j.cej.2017.12.119
- Dao, T. B. T., Ha, T. T. L., Do Nguyen, T., Nhien Le, H., Ha-Thuc, C. N., Nguyen, T. M. L., et al. (2021). Effectiveness of photocatalysis of MMT-supported TiO₂ and TiO₂ nanotubes for rhodamine B degradation. *Chemosphere* 280, 130802. doi:10.1016/j.chemosphere.2021.130802
- Dong, B., Li, F., and Feng, S. (2022). A visible-IR responsive BiVO₄/TiO₂ photoanode with multi-effect point defects for photothermal enhancement of photoelectrochemical water splitting. *Chem. Commun.* 58 (10), 1621–1624. doi:10.1039/d1cc04572e
- El-Kousy, S. M., El-Shorbagy, H. G., and Abd El-Ghaffar, M. (2020). Chitosan/montmorillonite composites for fast removal of methylene blue from aqueous solutions. *Mater. Chem. Phys.* 254, 123236. doi:10.1016/j.matchemphys.2020.123236
- Foroutan, R., Mohammadi, R., MousaKhanloo, F., Sahebi, S., Ramavandi, B., Kumar, P. S., et al. (2020). Performance of montmorillonite/graphene oxide/CoFe₂O₄ as a magnetic and recyclable nanocomposite for cleaning methyl violet dye-laden wastewater. *Adv. Powder Technol.* 31 (9), 3993–4004. doi:10.1016/j.apt.2020.08.001
- Jing, Y., Yin, H., Li, C., Chen, J., Wu, S., Liu, H., et al. (2022). Fabrication of Pt doped TiO₂-ZnO@ZIF-8 core@shell photocatalyst with enhanced activity for phenol degradation. *Environ. Res.* 203, 111819. doi:10.1016/j.envres.2021.111819
- Joshi, N. C., Congthak, R., and Gururani, P. (2020). Synthesis, adsorptive performances and photo-catalytic activity of graphene oxide/TiO₂ (GO/TiO₂) nanocomposite-based adsorbent. *Nanotechnol. Environ. Eng.* 5 (3), 21–13. doi:10.1007/s41204-020-00085-x
- Kočí, K., Matějová, L., Kozák, O., Capek, L., Vales, V., Reli, M., et al. (2014). ZnS/MMT nanocomposites: The effect of ZnS loading in MMT on the photocatalytic reduction of carbon dioxide. *Appl. Catal. B Environ.* 158, 410–417. doi:10.1016/j.apcatb.2014.04.048
- Kumar, R., Bhattacharya, S., and Sharma, P. (2021). Novel insights into adsorption of heavy metal ions using magnetic graphene composites. *J. Environ. Chem. Eng.* 9 (5), 106212. doi:10.1016/j.jece.2021.106212
- Laysandra, L., Sari, M. W. M. K., Soetaredjo, F. E., Foe, K., Putro, J. N., Kurniawan, A., et al. (2017). Adsorption and photocatalytic performance of bentonite-titanium dioxide composites for methylene blue and rhodamine B decoloration. *Heliyon* 3 (12), e00488.
- Lee, E., Lee, D., Yoon, J., Yin, Y., Lee, Y., Uprety, S., et al. (2018). Enhanced gas-sensing performance of GO/TiO₂ composite by photocatalysis. *Sensors* 18 (10), 3334. doi:10.3390/s18103334
- Li, J.-q., Zhou, Z.-w., Li, X., Yang, Y. L., Gao, J. f., Yu, R., et al. (2022). Synergistically boosting sulfamerazine degradation via activation of peroxydisulfate by photocatalysis of Bi₂O₃-TiO₂/PAC under visible light irradiation. *Chem. Eng. J.* 428, 132613. doi:10.1016/j.cej.2021.132613
- Li, X., Chen, Y., Tao, Y., Shen, L., Xu, Z., Bian, Z., et al. (2022). Challenges of photocatalysis and their coping strategies. *Chem. Catal.* 2, 1315–1345. doi:10.1016/j.cheat.2022.04.007
- Liao, W., Zhao, M., Rong, H., Jiang, P., Liao, Q., Zhang, C., et al. (2022). Photocatalyst immobilized by hydrogel, efficient degradation and self-regeneration: A review. *Mater. Sci. Semicond. Process.* 150, 106929. doi:10.1016/j.mssp.2022.106929
- Lin, J., Hu, H., Gao, N., Ye, J., Chen, Y., and Ou, H. (2020). Fabrication of GO@MIL-101 (Fe) for enhanced visible-light photocatalysis degradation of organophosphorus contaminant. *J. Water Process Eng.* 33, 101010. doi:10.1016/j.jwpe.2019.101010
- Lincho, J., Gomes, J., Kobylanski, M., Bajorowicz, B., Zaleska-Medynska, A., and Martins, R. C. (2021). TiO₂ nanotube catalysts for parabens mixture degradation by photocatalysis and ozone-based technologies. *Process Saf. Environ. Prot.* 152, 601–613. doi:10.1016/j.psep.2021.06.044

investigation, writing—review and editing. MW: resources, writing—review and editing, supervision, project administration, funding acquisition.

Funding

General Project of Science Research Foundation of Liaoning Province (LJKZ0363) and Central Government Guiding Local Project of Science and Technology Development Foundation (2022JH6/100100047).

Conflict of interest

The authors declare that the research was conducted in the absence of any commercial or financial relationships that could be construed as a potential conflict of interest.

Publisher's note

All claims expressed in this article are solely those of the authors and do not necessarily represent those of their affiliated organizations, or those of the publisher, the editors and the reviewers. Any product that may be evaluated in this article, or claim that may be made by its manufacturer, is not guaranteed or endorsed by the publisher.

Supplementary material

The Supplementary Material for this article can be found online at: <https://www.frontiersin.org/articles/10.3389/fchem.2023.1113186/full#supplementary-material>

- Liu, K., Zhang, H., Fu, T., Wang, L., Tang, R., Tong, Z., et al. (2022). Construction of BiOBr/Ti₃C₂/exfoliated montmorillonite Schottky junction: New insights into exfoliated montmorillonite for inducing MXene oxygen functionalization and enhancing photocatalytic activity. *Chem. Eng. J.* 438, 135609. doi:10.1016/j.cej.2022.135609
- Liu, S., Su, Z. L., Liu, Y., Yi, L. Y., and Chen, Z. L. (2021). Mechanism and purification effect of photocatalytic wastewater treatment using graphene oxide-doped titanium dioxide composite nanomaterials. *Water* 13 (14), 1915. doi:10.3390/w13141915
- Mallik, A., Roy, I., Chalapathi, D., Narayana, C., Das, T., Bhattacharya, A., et al. (2021). Single step synthesis of reduced graphene oxide/SnO₂ nanocomposites for potential optical and semiconductor applications. *Mater. Sci. Eng. B* 264, 114938. doi:10.1016/j.mseb.2020.114938
- Mottola, S., Mancuso, A., Sacco, O., De Marco, I., and Vaiano, V. (2022). Production of hybrid TiO₂/β-CD photocatalysts by supercritical antisolvent micronization for UV light-driven degradation of azo dyes. *J. Supercrit. Fluids* 188, 105695. doi:10.1016/j.supflu.2022.105695
- Nadali, A., Leili, M., Afkhami, A., Bahrami, A., and Karami, M. (2021). Synthesize and application of magnetic molecularly imprinted polymers (mag-MIPs) to extract 1-Aminopyrene from the human urine sample. *J. Environ. Chem. Eng.* 9 (5), 106253. doi:10.1016/j.jece.2021.106253
- Olea, M. A. U., Bueno, J. d. J. P., and Pérez, A. X. M. (2021). Nanometric and surface properties of semiconductors correlated to photocatalysis and photoelectrocatalysis applied to organic pollutants—A review. *J. Environ. Chem. Eng.* 9 (6), 106480. doi:10.1016/j.jece.2021.106480
- Paiva, J. P., Santos, B. A., Kibwila, D. M., Goncalves, T. C., Pinto, A. V., Rodrigues, C. R., et al. (2014). Titanium dioxide–montmorillonite nanocomposite as photoprotective agent against ultraviolet B radiation-induced mutagenesis in *Saccharomyces cerevisiae*: A potential candidate for safer sunscreens. *J. Pharm. Sci.* 103 (8), 2539–2545. doi:10.1002/jps.24057
- Pu, Z., Lan, Q., Li, Y., Liu, S., Yu, D., and Lv, X. J. (2019). Preparation of W-doped hierarchical porous Li₄Ti₅O₁₂/brookite nanocomposites for high rate lithium ion batteries at –20° C. *J. Power Sources* 437, 226890. doi:10.1016/j.jpowsour.2019.226890
- Sharma, M., Behl, K., Nigam, S., and Joshi, M. (2018). TiO₂-GO nanocomposite for photocatalysis and environmental applications: A green synthesis approach. *Vacuum* 156, 434–439. doi:10.1016/j.vacuum.2018.08.009
- Tahir, M. (2017). Ni/MMT-promoted TiO₂ nanocatalyst for dynamic photocatalytic H₂ and hydrocarbons production from ethanol-water mixture under UV-light. *Int. J. Hydrogen Energy* 42 (47), 28309–28326. doi:10.1016/j.ijhydene.2017.09.116
- Tao, E., Ma, D., Yang, S., and Hao, X. (2020). Graphene oxide-montmorillonite/sodium alginate aerogel beads for selective adsorption of methylene blue in wastewater. *J. Alloys Compd.* 832, 154833. doi:10.1016/j.jallcom.2020.154833
- Umer, M., Tahir, M., Azam, M. U., and Jaffar, M. M. (2019). Metals free MWCNTs@TiO₂@MMT heterojunction composite with MMT as a mediator for fast charges separation towards visible light driven photocatalytic hydrogen evolution. *Appl. Surf. Sci.* 463, 747–757. doi:10.1016/j.apsusc.2018.08.240
- Wang, J., Zhao, X., Wu, F., Tang, Z., Zhao, T., Niu, L., et al. (2021). Impact of montmorillonite clay on the homo- and heteroaggregation of titanium dioxide nanoparticles (nTiO₂) in synthetic and natural waters. *Sci. Total Environ.* 784, 147019. doi:10.1016/j.scitotenv.2021.147019
- Wang, Q., Wang, X., Li, X., Cai, Y., and Wei, Q. (2011). Surface modification of PMMA/O-MMT composite microfibers by TiO₂ coating. *Appl. Surf. Sci.* 258 (1), 98–102. doi:10.1016/j.apsusc.2011.08.013
- Wang, W., Xu, H., Ren, X., and Deng, L. (2019). Interfacial interaction of graphene oxide with Na-montmorillonite and its effect on the U (VI) retention properties of Na-montmorillonite. *J. Mol. Liq.* 276, 919–926. doi:10.1016/j.molliq.2018.12.130
- Wang, Z., Li, Y., Cheng, Q., Wang, X., Wang, J., and Zhang, G. (2022). Sb-Based photocatalysts for degradation of organic pollutants: A review. *J. Clean. Prod.* 367, 133060. doi:10.1016/j.jclepro.2022.133060
- Xiang, H., Tuo, B., Tian, J., Hu, K., Wang, J., Cheng, J., et al. (2021). Preparation and photocatalytic properties of Bi-doped TiO₂/montmorillonite composite. *Opt. Mater.* 117, 111137. doi:10.1016/j.optmat.2021.111137
- Xu, X., and Li, D. (2022). Ligand-Decomposition assistant formation of CdS/TiO₂ hybrid nanostructure with enhanced photocatalytic activity. *J. Alloys Compd.* 914, 165393. doi:10.1016/j.jallcom.2022.165393
- Yadav, M., and Ahmad, S. (2015). Montmorillonite/graphene oxide/chitosan composite: Synthesis, characterization and properties. *Int. J. Biol. Macromol.* 79, 923–933. doi:10.1016/j.ijbiomac.2015.05.055
- Yang, Y., Yu, W., He, S., Yu, S., Chen, Y., Lu, L., et al. (2019). Rapid adsorption of cationic dye-methylene blue on the modified montmorillonite/graphene oxide composites. *Appl. Clay Sci.* 168, 304–311. doi:10.1016/j.clay.2018.11.013
- Yang, Z., Yuan, Z., Shang, Z., and Ye, S. (2020). Multi-functional membrane based on montmorillonite/graphene oxide nanocomposites with high actuating performance and wastewater purification. *Appl. Clay Sci.* 197, 105781. doi:10.1016/j.clay.2020.105781
- Yin, J. Y., Boaretti, C., Lorenzetti, A., Martucci, A., Roso, M., and Modesti, M. (2022). Effects of solvent and electrospinning parameters on the morphology and piezoelectric properties of PVDF nanofibrous membrane. *Nanomaterials* 12 (6), 962. doi:10.3390/nano12060962